Control of Particle Morphology and Film Structures of Carboxylated Poly(Methyl Methacrylate)/Poly (*n*-Butylacrylate) Composite Latex Particles

S. Kirsch,[1] J. Stubbs,[2] J. Leuninger,[1] A. Pfau,[3] D. Sundberg[2]

[1]*BASF AG, Product Development EDK/D, D-67056 Ludwigshafen, Germany*
[2]*University of New Hampshire, Polymer Research Group, Materials Science Program, Durham, New Hempshire 03824, USA*
[3]*BASF AG, Marketing PSA EDK/KH, H201, D-67056 Ludwigshafen, Germany*

Received 28 February 2003; accepted 20 August 2003

ABSTRACT: Particles with a hard core of 66% poly(methyl methacrylate)/34% poly(*n*-butyl acrylate) copolymer and a soft shell of pure poly(*n*-butyl acrylate) were synthesized via a two-stage emulsion polymerization process. The particle morphology and the surface structure of the dispersion films were analyzed by atomic force microscopy (AFM). The results, concerning single particle structure and the corresponding films, are correlated to macroscopic properties similar to the minimum expected from the kinetic side. The different morphologies are compared to the findings reported in a previous article, where the corresponding soft-core/hard-shell dispersions were analyzed (Kirsch et al. Colloid Surf A 2001, 183–185, 725). The key parameters to tailor the particle morphology are thermodynamic factors, for example: (i) the stage ratio and (ii) the phase compatibility and kinetic factors affecting the polymer chain mobility (e.g., cross-linking and polymer glass transition temperature). In this work, we used a core material which is in the glassy state at room temperature, however, above the polymer glass temperature (T_g) at polymerization temperature. The diffusion of the second-stage polymer chains is therefore strongly affected. From this point of view, the major influence for the current system is expected from the kinetic side. The different morphologies of the single particles are discussed qualitatively and the effects of reaction parameters and our results from previous work are compared to the results of computer simulation work and other results.
© 2003 Wiley Periodicals, Inc. J Appl Polym Sci 91: 2610–2623, 2004

Key words: emulsion polymerization; latex; simulation; morphology; atomic force microscopy

INTRODUCTION

The applications of polymer latices often require special attention toward the particle morphology of composite latex particles. These types of particles are widely used in modern, water-based, industrial applications such as paints,[1,2] coatings, and adhesives. By using a tailored particle morphology, latex film properties can be achieved which are not accessible by physically blending of two or more different polymer components. In addition, special interaction phenomena of phase-separated particles to various substrates may occur.[3,4]

Consequently it has become of great interest to understand how particle morphology can be controlled. The most common process to synthesize composite latex particles is via a two-step emulsion polymerization. This, on the first glance a simple process, comprises a complex variety of process parameters (e.g., reaction temperature, feeding time of the reactants, and feeding sequences). The use of different monomers at different stages in the emulsion polymerization process allows one to achieve complex particle morphologies. Parameters to be considered in controlling the particle morphology can be divided into the following two types:

(1) Thermodynamic factors: the equilibrium morphology determines the resulting structure. The most important parameter is to take advantage of the contribution of the surface-free energy. The surface-free energy can be affected by the type of monomer used during polymerization,[5] the stage ratio,[6] the type and amount of surfactant used for polymerization,[7,8] and the type and amount of initiator.[9,10] Quantitative guidelines and methods to predict the equilibrium morphology are reported elsewhere.[11,12]
(2) Kinetic factors: the resulting particle morphology is controlled by diffusion and phase rearrangement within the particles. The mobility of the polymer chains is restricted and hence phase separation and rearrangement is slower than the polymerization rate. The mobility of the radical chains can be strongly affected by crosslink-

Correspondence to: S. Kirsch (stefan.01.kirsch@basf-ag.de).
Contract grant sponsor: University of New Hampshire Latex Morphology Industrial Consortium.

Journal of Applied Polymer Science, Vol. 91, 2610–2623 (2004)
© 2003 Wiley Periodicals, Inc.

ing,[13] the monomer concentration within the particles, and hence, monomer feed strategy, polymer glass transition temperature (T_g), and reaction temperature. A computational approach is given in ref. 14.

The effect of carboxylic acids can neither be attributed to the thermodynamic nor to the kinetic factors alone. In fact, they affect morphology through both considerations. It is known that the radical flux (entry and exit) is affected by the surface layer of carboxylic acid on a dispersion particle.[15] In addition, the length of entering radicals is increased when acid comonomers are used, and this reduces their ability to diffuse into the seed particles. On the other hand, surface-free energy, and therefore, the equilibrium morphology,[6,16,17] between polymer phases are also modified when hydrophilic groups (e.g., acid comonomers or sulfate groups from the initiator), are incorporated into the polymer chains.

In contrast to ref. 18 in the current work, a conventional emulsion polymerization process was used to synthesize a hard seed particle of carboxylated poly(methyl methacrylate) (PMMA)/poly(*n*-butyl acrylate) (PBA) (66 : 34). In a second stage, pure PBA is polymerized as a soft shell. The phase ratio of soft-to-hard (s/h) was varied over a wide range. Furthermore, the effect of acrylic acid and crosslinking of the shell material was also investigated. One important aspect of this work was to correlate the particle morphology to (1) the results of simulation work by using software developed at the University of New Hampshire called UNHLATEX™ EQMORPH[19] and UNHLATEX™ KMORPH[20,21] and (2) macroscopic properties of the dispersion film. For the latter, the ability to form a film is characterized by the minimum film-forming temperature (MFFT) and film surface properties are characterized via pendulum hardness and film gloss measurements.

Different characterization tools are available to characterize the particle morphology of latex particles. Beside scattering techniques,[13] analytical ultracentifugation,[13] and NMR techniques,[6] different microscopic techniques[6,18] are most common to analyze the particle structure. Atomic force microscopy (AFM) was used to characterize the current latex system due to the following advantages: (1) it is possible to map the topography at surfaces; (2) it is possible to map a material contrast, by taking advantage of differences in viscoelastic properties of different phases by using phase imaging,[22,23] and (3) spatial resolutions below 10 nm can be routinely achieved on the investigated polymer system.

The effects of the different reaction parameters such as phase ratio, phase compatibility, crosslinking, and acrylic acid on the particle morphology were investigated. The findings are compared to the results we presented in ref. 18, where the same chemistry but the opposite T_g sequence, that means soft core/hard shell, was used.

EXPERIMENTAL

Equipment

All syntheses were performed in a 2000-ml four-necked flask equipped with a reflux condenser, N_2 gas inlet tube, anchor-stirrer stirring at 120 rpm, inlet tubes to feed the preemulsions, and a feeding tube for the initiator solution.

The particle size and particle-size distribution were measured via dynamic light scattering (DLS) and capillary hydrodynamic fractionation (CHDF). For DLS measurement, the dispersions were diluted to 0.005–0.01 wt %. Measurements were performed at 23°C with an IIC particle sizer (Malvern Instruments). Number-averaged diameters obtained by fitting the intensity autocorrelation function according ISO-Norm 13 321 are reported. All samples for CHDF (1100, Matec Applied Science) were prepared by diluting the original sample to 1% solid. All samples were passed through a 1.2-μm filter (Millipore). The diameters were recorded as number-averaged diameters.

All AFM data presented here were recorded in the tapping mode with a Nanoscope Dimension 3000 SPM (Digital Instruments) capable of recording phase images and using Si cantilevers (35 N/m, ν_0 approx. 300 kHz, Nanoprobe). The sample preparation for AFM measurements is described elsewhere.[18]

Synthesis and particle characterization

The P(BA/MMA) composite latex particles were prepared by a conventional semibatch emulsion polymerization process. The recipe for the standard 75 hard phase/25 soft particles is described below. The recipes for the variations can be calculated from the data given in Table I.

For the hard P(MMA/BA) seed particles, 26 g of the first-stage material (see below), 351 g deionized (DI) water, 6.5 g of a 15 wt % of aqueous solution of SDS, and 13 g of the initiator solution (0.545 mM aqueous solution of NaPS) was reacted at 85°C for 15 min. The first-stage preemulsion (columns 2–6 in Table I) was prepared from 198 g water, 82 g SDS solution, 4.81 g acrylic acid, 317 g MMA, and 171 g nBA. The preemulsion and 50 g initiator solution were fed for 2 h to the reaction mixture.

The second-stage preemulsion (columns 7–11 in Table I) consisted of 75 g water, 9 g SDS solution, 4.81 g acrylic acid, and 163 g nBA. The second-stage material was fed after the end of the first stage with 17 g initiator solution for another 45 min into the reaction vessel. The pH during the polymerization process was 2–3.

TABLE I
Chemical Composition of the First- and Second-Stage Polymerization and Final Particle Size

Sample—Hard/soft wt %	First stage preemulsion					Second stage preemulsion					Characterization		
	Water (g)	SLS (g)	AA (g)	MMA (g)	BA (g)	Water (g)	SLS (g)	AA (g)	MMA (g)	BA (g)	Solids (%)	DSL d (nm)	CHDF d (nm)
I75/0	198	57	4.81	317	171	—	—	—	—	—	46	114	—
I25/75	134	57	1.6	106	57	139	35	8.78	—	488	44.5	94	86
I50/50	136	57	3.25	211	114	137	35	7.15	—	325	44.4	127	118
I75/25	198	82	4.81	317	171	75	9	4.81	—	163	44.7	127	123
I75/25wo	192	82	—	317	171	70	9	—	—	163	44.8	136	131
I75a3/25	216	82	19.5	317	171	70	9	—	—	163	44.5	135	93
I75/25a3	192	82	—	317	171	93	9	19.5	—	163	44	130	—
I75/25c[a]	195	82	4.81	317	171	77	9	4.81	—	163	45.2	136	119
I75p/25	198	82	4.81	487	—	75	9	4.81	—	163	44.6	85	62
I50p/50	85	10	5.6	369	—	235	95	5.6	122	247	44.6	181	—
I35p/65	85	10	5.6	257	—	235	95	5.6	157	325	44.8	125	—
I25p/75	85	10	5.6	182	—	235	95	5.6	182	375	45	117	—

[a] Second stage crosslinked by EGDMA.

After the polymerization, the dispersions were neutralized with NH_3 to pH 7 and then allowed to cool down to room temperature (RT).

Characterization of dispersion films

The MFFT was measured according to ISO 2115 plastics. The pendulum hardness was determined according to DIN 53157 from a 200 μm (wet) film after 24 h drying time. Gloss was measured on a 200 μm (wet) film after 24 h drying time with a BYK-Gardener Micro TRI Gloss meter.

RESULTS AND DISCUSSION

Simulations

Simulations were performed to predict the expected particle morphologies by using software developed at the University of New Hampshire. Two software packages were used, UNHLATEX™ EQMORPH,[19] which predicts the equilibrium morphology developed under conditions of thermodynamic control, and UNHLATEX™ KMORPH,[20,21] which determines if nonequilibrium morphologies may develop due to kinetic control. The equilibrium predictions will be described first.

The EQMORPH software determines the morphology that will be formed if the system is able to achieve a state of thermodynamic equilibrium. This state is one that minimizes the surface-free energy of the structured particle, and is thus dependent on the interfacial tensions at the various interfaces within the particle [seed polymer/water ($\gamma_{P1/W}$), second-stage polymer/water ($\gamma_{P2/W}$), and seed polymer/second-stage polymer ($\gamma_{P1/P2}$)]. The equations to calculate the surface-free energy have been reviewed extensively in the literature.[7,19,24] In the EQMORPH software, a so-called topology map, shown in Figure 1(A), is used to classify the full spectrum of possible equilibrium morphologies. The Gibbs free energy associated with making each of these morphologies is then calculated for a given system and plotted to create an energy surface, as shown in Figure 1(B). The minimum point on this surface corresponds to the morphology on the map having the least energy, which is the predicted equilibrium morphology. The interfacial tensions are calculated as a function of the polymer types, surfactant concentration, initiator and buffer concentrations (ionic strength of the aqueous phase affects the surfactant partitioning), acid comonomer levels, temperature, and the charge density of the polymer surface.

In the first article in this series,[18] simulations were performed and it was noted that the software was not fully capable of making predictions in cases containing acid comonomers. In that case, certain assumptions were made to simulate the incorporation of acid comonomers. Since that time, the program has been expanded so that it is now capable of handling these types of systems without having to make these assumptions. From a thermodynamic standpoint, the effect on morphology development of incorporating acid comonomers into the seed or second-stage polymer is to increase the polarity of that phase. This decreases the interfacial tension of that polymer against the water phase and may make it more favorable to produce a morphology in which that polymer is in contact with the water phase (i.e., on the particle surface to some extent). Because the polarity of that polymer is affected, this will also impact the interfacial tension at the interface between the seed and second-stage polymers, and this may also affect the morphology. EQMORPH considers the effect of acid comonomers by calculating the decrease in the interfacial tension of the polymer against water based on measurements made in our laboratory at the University of New Hampshire for the interfacial tension be-

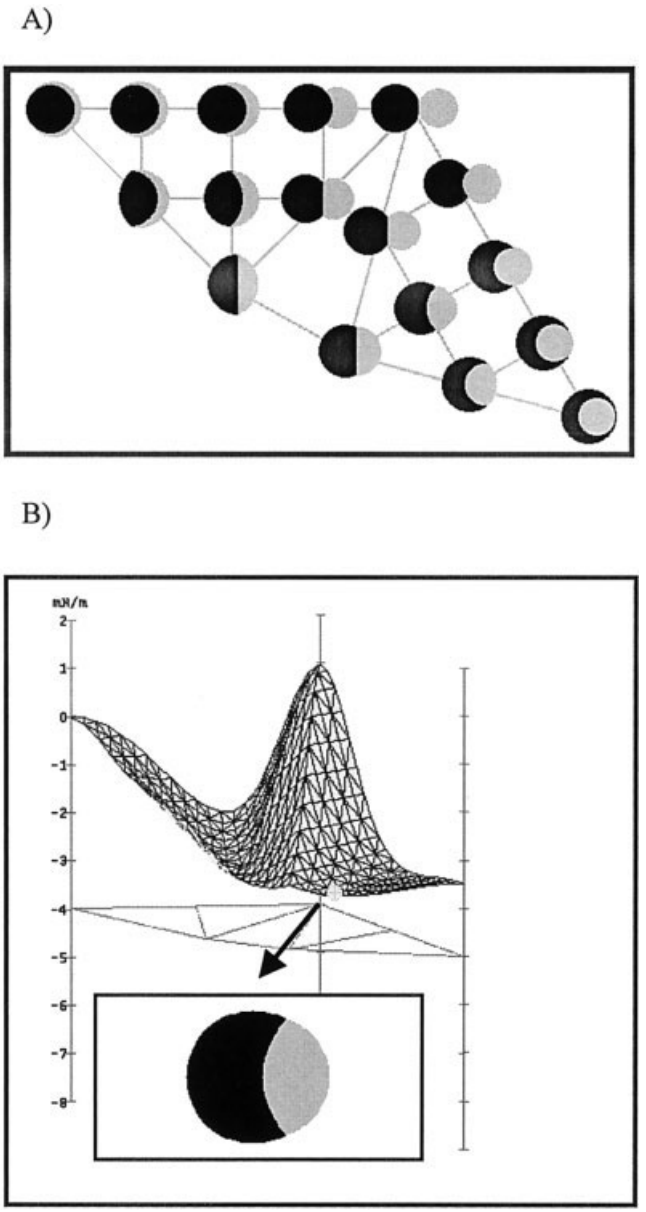

Figure 1 (A) Base topology map for possible equilibrium morphologies ranging from core shell (upper left) to inverted core shell (lower right). (B) The corresponding energy surface for experiment I75/25wo. The minimum energy on the energy surface indicates the point on the base topology map where the predicted morphology is located, shown for this case in the lower right-hand corner of (B).

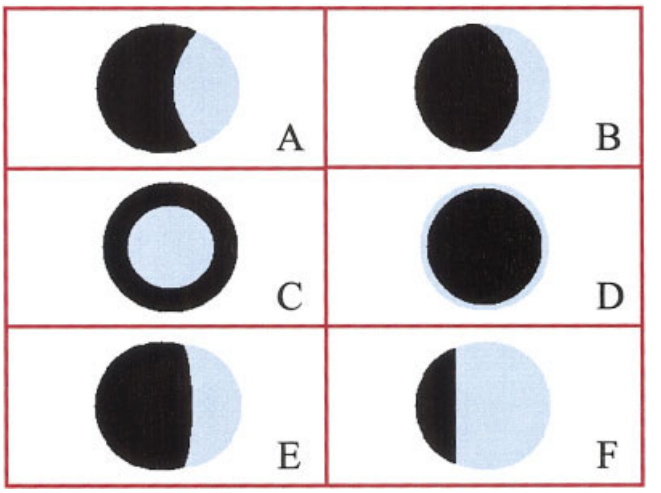

Figure 2 Predicted equilibrium morphologies for representative experiments. (A) I75/25wo, (B) I75/25, (C) I75a3/25, (D) I75/25a3, (E) I75p/25, (F) I25/75. Dark phase is the first-stage, soft-phase material.

tween water and copolymers of styrene/methacrylic acid and butyl acrylate/methacrylic acid.

Predictions of the equilibrium morphology were made for several representative experiments and are shown in Figure 2 (dark area is the seed polymer and the light area is the second stage). The interfacial tension values used to compute these predicted morphologies are listed in Table II. The polymer/water values were determined by adjusting the interfacial tensions of the pure polymers against water[25] and adjusting them to account for the effect of SDS surfactant and acid comonomers (based on unpublished data obtained within our laboratory). The polymer/polymer values are estimated by using the harmonic mean equation.[26] Figure 2(A) represents experiment I75/25wo, in which the seed is a copolymer of BA and MMA and the second stage is pure PBA, with no acrylic acid (AA) incorporated in either stage. The predicted morphology is a hemisphere in which the seed polymer partially engulfs the second-stage PBA. The reason for this partial engulfment is that MMA is sufficiently more polar than BA, so that the interfacial tension of the seed against water is less than for the second stage against water. Therefore, the seed polymer tends to cover more of the particle surface. The reason that the seed polymer does not fully cover the second stage, producing an inverted core-shell morphology, is due to the fairly high surfactant concentrations used in these experiments. The particle surfaces have a significant amount of adsorbed surfactant and this has the effect of decreasing the polymer/water interfacial tensions. Because more nonpolar surfaces adsorb more surfactant, this effect is greater on the more nonpolar surface. This decreases the differ-

TABLE II
Interfacial Tension Values Used to Predict the Equilibrium Morphologies in Figure 2

Experiment	$\gamma_{P1/w}$ (mN/m)	$\gamma_{P2/W}$ (mN/m)	$\gamma_{P1/P2}$ (mN/m)
I75/25wo	13.9	15.4	2.0
I75/25	12.0	10.4	2.0
I75a3/25	10.6	14.1	2.0
I75/25a3	12.6	9.3	2.0
I75p/25	11.3	10.0	3.2
I25/75	13.7	14.2	2.0

ence between the interfacial tensions at the seed polymer/water and second-stage polymer/water interfaces and makes the energy of the polymer/polymer interface more important in determining the morphology. The system then tends to decrease this interfacial area and forms a hemisphere morphology rather than an inverted core shell.

Figure 2(B) shows the predicted morphology for experiment I75/25, in which AA is incorporated into both stages. As calculated from Table I, there is actually a higher AA content in the second-stage polymer (2.9 wt % by) than in the seed polymer (1%). This causes the second stage, which was originally less polar than the seed when no AA was used, to become slightly more polar than the seed polymer and results in a predicted hemisphere-type morphology in which the second stage slightly engulfs the seed.

The morphology prediction for experiment I75a3/25 is shown in Figure 2(C). In this experiment, a higher level of AA is used in the seed, but none is used in the second stage. This causes the polarity of the seed to be significantly greater than the second-stage PBA and the predicted morphology is now an inverted core shell. This is opposed to the case in Figure 2(D) for experiment I75/25a3, where a high level of AA is used in the second stage but none is incorporated into the seed polymer. In this case, a core-shell morphology is predicted.

Figure 2(E) represents experiment I75p/25, in which AA is used in both stages but the seed contains only MMA instead of MMA and BA. This can be related to experiment I75/25 in Figure 2(B), except with the BA in the seed polymer removed. This effectively decreases the interfacial tension of the seed polymer against water, while at the same time increases the interfacial tension between the two polymers. The resulting morphology prediction is still a hemisphere, but with less engulfment of the seed polymer than for the case in Figure 2(B).

The last experiment simulated with EQMORPH is I25/75 [Fig. 2(F)], which is similar to I75/25 [Fig. 2(B)] but with a different stage ratio. Once again, a hemispheric morphology is predicted, but now the volume fraction of the hard seed polymer is greatly reduced.

Simulations were also performed by using the KMORPH software to determine if kinetic considerations may limit the development of the equilibrium morphologies predicted by using EQMORPH. It is known that the formation of nonequilibrium morphologies is due to slow diffusion rates within the seed particles, which prevent the second-stage polymer radicals from fully penetrating into the seed particles after entering from the water phase. This can prevent the morphology from reaching its equilibrium state. For example, when penetration is very limited, such as in a glassy seed polymer in a starve-fed reaction, core-shell morphologies will be formed even if they are not thermodynamically favored.

The KMORPH software simulates the kinetics of seeded emulsion polymerization to determine a probability density distribution for polymer radical termination events as a function of particle radius, which indicates the location within the particles where the majority of the second-stage polymer will be formed. This distribution is then used to construct a picture of the particle by placing domains of second-stage polymer within the seed particles at radial distances governed by the distribution. These simulated particles are displayed as if they were thin cross sections to give an idea of the internal morphology of the particles. It should be noted that the program does not consider thermodynamic driving forces for rearrangement of the second-stage polymer domains, but determines where they are formed in the particle based on the random diffusion process. Thus, in cases where diffusion of radicals and dead polymer chains occur very easily, the predictions of EQMORPH must be considered, and the morphology formed may be closer to the equilibrium state.

The simulation is dynamic and almost all parameters, other than some physical data (densities, etc.), change throughout the polymerization so it is not possible to list many of the parameters used in the simulation. Some of the most important parameters in the simulation are diffusion coefficients of polymer radicals as a function of radical chain length, as they are used to calculate both the depth of radical penetration into particles and the termination rate coefficients (which are always diffusion controlled). These values are estimated from the diffusion coefficient of the monomer and the chain length of the radical as described previously.[20] The method to estimate the monomer diffusion coefficients has also been described in detail.[27] Other than these values, the most important value is the propagation rate coefficient, k_p. An Arrhenius expression is used to describe the temperature dependence of k_p (derived from pulsed laser polymerization experiments), with a preexponential factor equal to 1.82×10^7 L/mol/s and an activation energy equal to 17.4 kJ/mol.[28] The models on which the program is based have been previously described in more detail.[20,21]

Simulations were performed for representative experiments, and the kinetic simulations showed that the monomer concentration within the particles throughout each of the reactions is very low, as is typical of semibatch polymerizations. The morphology predictions are shown in Figure 3. Figure 3(A) represents experiment I75/25wo, in which there is no AA present in either stage. In this case, the T_g of the P(BA-*co*-MMA) seed particles is about 51°C, which is significantly less than the reaction temperature. It is seen that the second-stage polymer radicals are able to diffuse fully to the particle center, and this results in a morphology in which domains of PBA (dark) are located throughout the particle. However, the radial

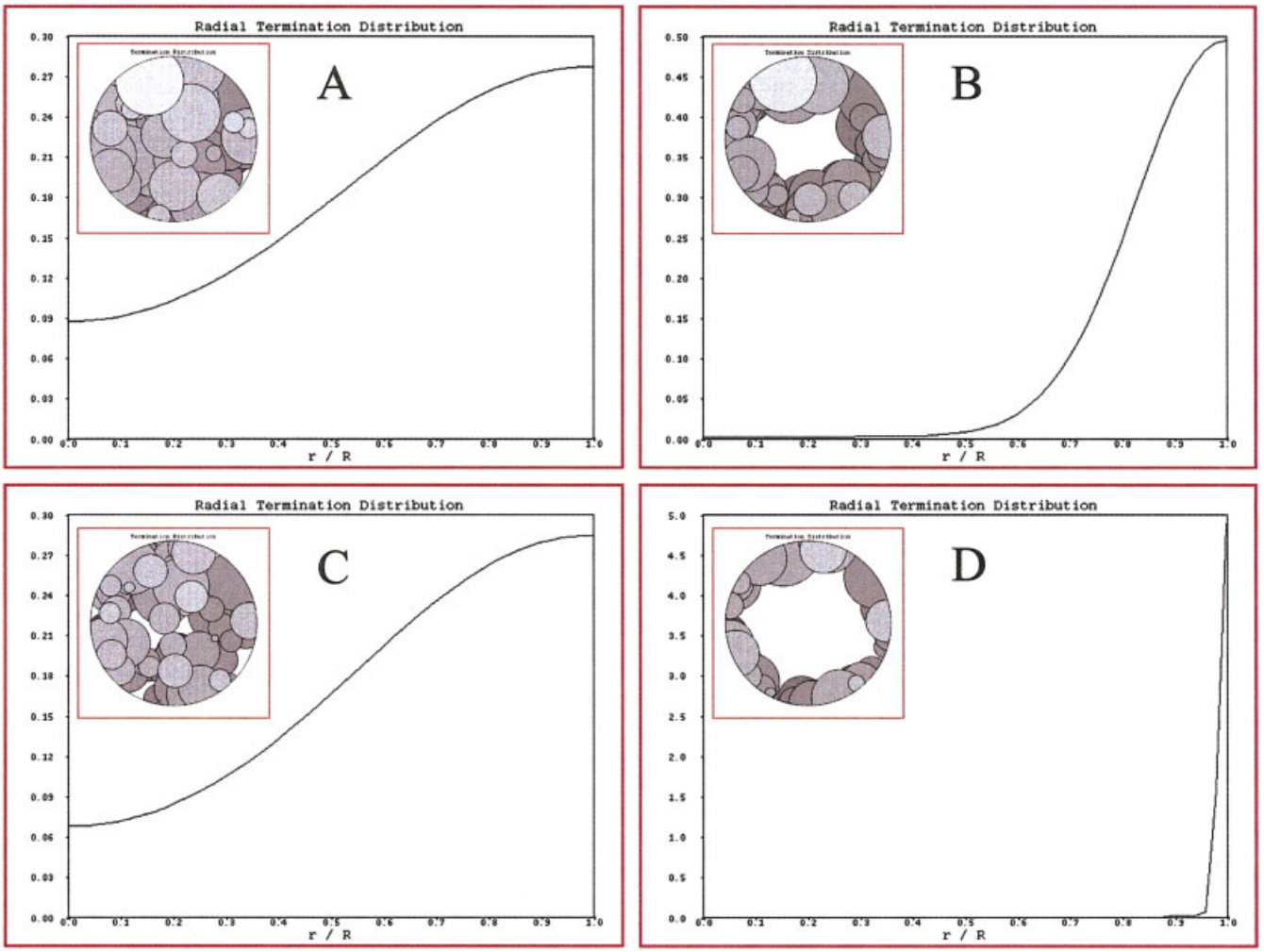

Figure 3 KMORPH simulations indicating kinetic limitations to morphology development. The graphs represent distributions of the probability density for termination events of the second-stage polymer radicals as a function of reduced radius within the particles. These distributions are used to generate the simulated particle cross sections in which the second-stage polymer is indicated as dark domains. The simulations correspond to the following conditions: (A) P(BA/MMA) seed, no acid comonomer in either stage; (B) P(BA/MMA) seed, acid comonomer in second stage only; (C) P(BA/MMA) seed, acid comonomer in both stages; (D) PMMA seed with acid comonomer in seed only.

distribution does predict a gradient in the concentration of the second-stage polymer, which is formed preferentially toward the outside of the particles. In a case such as this, although radical penetration is not highly restricted, there is likely to be some limitation to the rearrangement of the polymer phases so that the equilibrium morphology will not be fully developed.

The simulation for experiment I75/25a3 is shown in Figure 3(B), in which AA is used in the second stage but not in the seed. In terms of radical penetration, the most important effect of AA in the second stage is to significantly increase the length of the entering radicals. Therefore, the entering radicals will diffuse more slowly from the very beginning as compared to cases without AA in the second stage. For the simulation of this experiment, the oligomeric radicals enter the particles with a length of 10 monomer units, as opposed to 2 units for PBA radicals in the absence of AA. This length is based on estimates made by Dong and Sundberg.[29] The distribution in Figure 3(B) shows that the extent of radical penetration is reduced compared to the case in Figure 3(A). They are still able to penetrate to a significant depth, but essentially none of the second-stage polymer should be formed within the inner 50% of the particle radius.

Figure 3(C) represents an experiment in which AA is used in both stages. The simulation was modeled after experiment I75/25, but it represents conditions similar to those in other experiments as well (I50/50 and I25/75, although the seed particle diameters are smaller in these experiments, which will increase the fraction of the particle radius that the radicals can penetrate). The effect of AA in the seed polymer is to allow the seed to be slightly swollen with water and results in a decrease in its glass transition temperature in the wet state. This effect was shown clearly by Lee

et al.[30] by measuring the T_g's of acid-containing copolymers and terpolymers using a microcalorimeter. Based on the data presented in that articles, we estimated that the T_g of the P(BA-MMA-AA) seed polymer would be about 13°C lower in the wet state than its non-acid-containing counterpart. This lower T_g slightly softens the seed and allows increased penetration. This is shown in Figure 3(C) in which the distribution is similar to Figure 3(A). In this case, the lower T_g of the seed counteracted the longer lengths of the entering radicals due to the AA in the second stage, and essentially, full penetration is once again possible.

Figure 3(D) considers a case similar to I75p/25 in which the seed polymer is now only a copolymer of MMA and AA (without BA in the seed). It was estimated that the T_g of the seed in the wet state would be reduced by about 20°C and is equal to 99°C as opposed to 119°C for pure PMMA. Because the T_g is greater than the reaction temperature and the monomer concentration is very low, the seed polymer is glassy during the reaction. Therefore, the diffusion rates are very slow and penetration is extremely limited. Figure 3(D) predicts that the second-stage polymer should be formed only at the outside of the particles. Simulations for these conditions are not sensitive to the use of AA in the second stage because longer entering radicals would only further decrease the level of penetration, which is already extremely limited without AA in the second stage.

It is noted that simulations have not been performed for the conditions of I75a3/25, when AA is used in the seed but not in the second stage. However, it is easy to imagine what the result would be in this case. This can be compared to Figure 3(C) in which acid is used in both stages, but the level of penetration would be increased even further because of the shorter entering radicals. This would result in a radial distribution that is flatter than in Figure 3(C) with even more second-stage polymer formed in the center of the particles.

Finally, simulations were also not performed for experiment I75/25c, in which crosslinking was incorporated in the second stage, because the software is not yet able to model this effect. One may guess that crosslinking would decrease the level of penetration by increasing the molecular weight of the second-stage polymer. However, this would only be effective if radicals experienced crosslinking reactions before reaching the interior of the particles. If they were able to first penetrate and then were crosslinked, they may actually become trapped within the particles because of excessive chain entanglements, much like an interpenetrating network (IPN). More experimentation is required to understand this effect before it can be properly incorporated into the model, and this is part of our ongoing research.

At this point, it is useful to consider the thermodynamic (EQMORPH) and kinetic (KMORPH) simulations collectively, to make an overall judgement for the type of morphology that is expected in each experiment.

I75/25 wo

The kinetic simulation result in Figure 3(A) corresponds to experiment I75/25wo and shows that full penetration of the second-stage polymer into the seed particles is possible. However, the fact that there is a slightly higher probability to form second-stage polymer toward the outer region of the particles suggests that diffusion is somewhat restricted. This indicates that the equilibrium morphology, as predicted in Figure 2(A), may not be fully developed. The equilibrium prediction in Figure 2(A) suggests that both polymers will make up some part of the external particle surface, but that the seed polymer will slightly engulf the second stage. Because the kinetic simulations predict that penetration is possible, it should be possible for this partial engulfment to occur. However, the diffusional restrictions may result in the formation of multiple partially engulfed domains of second-stage polymer near the surface, rather than only one large domain, as indicated in Figure 2(A). It is also possible that some domains may be formed within the interior of the particles and may then be kinetically prevented from migrating back toward the particle surface.

I75/25, I50/50, and I25/75

The kinetic simulation in Figure 3(C) represents the experiments, in which acid comonomer was incorporated in both stages, such as I75/25, I50/50, and I25/75. As for experiment I75/25wo [Fig. 3(A)] discussed above, full penetration is possible, but diffusion is somewhat restricted so that the equilibrium morphology is not likely to fully develop. Figure 2(B) predicts a similar equilibrium morphology as predicted for I75/25wo in Figure 2(A), but that now the second stage should partially engulf the seed polymer. Therefore, the situation should be similar to that described above for I75/25wo, except that the second stage should spread slightly more on the particle surface, rather than being partially engulfed by the seed polymer. Once again, it would not be surprising if multiple domains were formed on the surface as well as some internal occlusions within the particle, due to the diffusional limitations to phase rearrangement. For the experiments with greater ratios of second-stage polymer (I50/50 and I25/75), the second stage should make up an even larger portion of the particle surface, as depicted by Figure 2(F).

I75/25a3 and I75a3/25

The kinetic simulation result in Figure 3(B) represents an experiment with AA only present in the second

stage and shows that penetration is more restricted than in experiment I75/25wo. Some level of penetration is possible, to about 50% of the particle radius, but the second-stage polymer will be formed only in the outer region of the particles. The EQMORPH prediction in Figure 2(B) is a core shell. Therefore, it is likely that a core-shell structure will be produced in this experiment, because both the thermodynamic and the kinetic factors favor this type of morphology. A kinetic simulation was not performed for experiment I75a3/25, but as discussed above, full penetration is possible, and to an even greater extent than predicted for Experiment I75/25 [Fig. 3(C)]. The predicted equilibrium morphology is an inverted core shell, as shown in Figure 2(C). Therefore, the likely structure in this case will be an inverted core-shell morphology or a completely occluded morphology, in which the second-stage polymer is completely engulfed by the seed polymer.

I75p/25

Figure 3(D) represents the kinetic simulation for experiment I75p/25 with pure PMMA as seed particle. It shows that penetration is greatly restricted for this experiment, and therefore, it is very likely that a core-shell morphology will be formed. The equilibrium prediction is a hemisphere morphology, represented by Figure 2(E). This morphology, although thermodynamically favored, is not likely to be formed because of the strong kinetic restrictions to penetration into the seed particles. However, the fact that the equilibrium morphology is a hemisphere also means that there is not a large driving force to place one polymer on the surface rather than the other. Given this, it is likely that a core-shell morphology will be formed, as driven by the kinetic factors which will control the morphology development.

Particle morphology

AFM was used to characterize the morphology of single particles. The sample preparation is described in detail in ref. 18. In the following, AFM measurements were done on well-separated dispersion particles or monolayer of dispersion particles mapped at room temperature under ambient conditions.

Variation of phase ratio

In a first step, only the core material was characterized to judge whether morphology effects seen in the composite latex particles have their origin from a prestructured core. Figure 4 shows the AFM phase image of the hard-phase core material sample I75/0. No material contrast is expected nor could be detected. The seed particles are very uniform and could be assumed to be spherical before drying in their shape. Therefore, no structural impact from the core material at the beginning of the second-stage polymerization process is expected. In other words, the probability of polymerizing nBA is the same at any point at the surface of the seed.

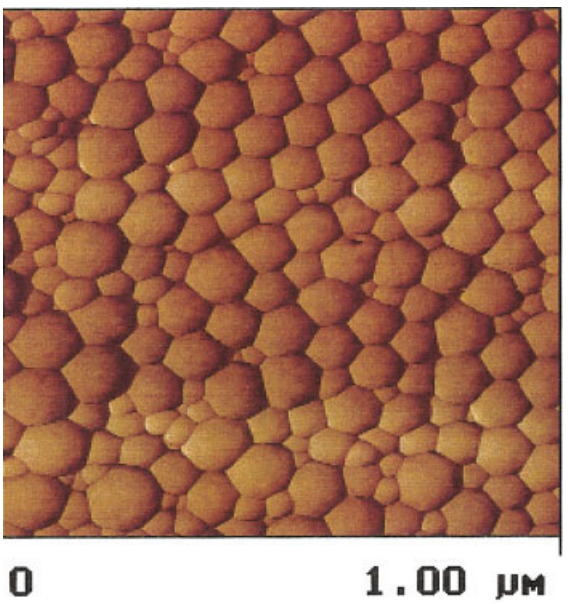

Figure 4 A phase image taken by AFM of the first-stage seed polymer on a field of view of 1×1 μm is shown.

In Figure 5(A–C), the results of the AFM phase images taken from the phase ratio variation series (see Table I, sample I75/25, I50/50, and I25/75) are shown. In the phase image, the hard phase of PMMA/PBA appears with a more positive phase shift as bright areas in the micrograph. The soft, pure PBA phase appears with a negative phase shift (i.e., with a dark contrast in the images). As already discussed in ref. 18, at the edges of the particles the topographic information is strongly present in the phase information, which can be seen from the dark shadows at the particles in Figure 5(A), for example.

In the first set of experiments, I75/25, I50/50, and I25/75 [Fig. 5(A–C)], the T_g of the hard phase is below polymerization temperature and is further decreased by partial swelling with water due to the presence of AA in the seed polymers. Therefore, a certain degree of polymer chain mobility is possible. In the case of small soft-phase content (I75/25), the soft phase forms isolated islands; thus, the structure looks like Dalmatians. The former seed is no longer spherical in shape and the soft phase seems to form bowls rather than being on top of the hard-phase core material. Whether the soft phase forms a continuous soft-phase core or not, cannot be distinguished from these images. From the thermodynamic point of view, the resulting structure may be due to the fact that there is not a dominant driving force for placing one polymer at the water interface rather than the other, so the system tends to decrease the polymer/polymer interfacial area. How-

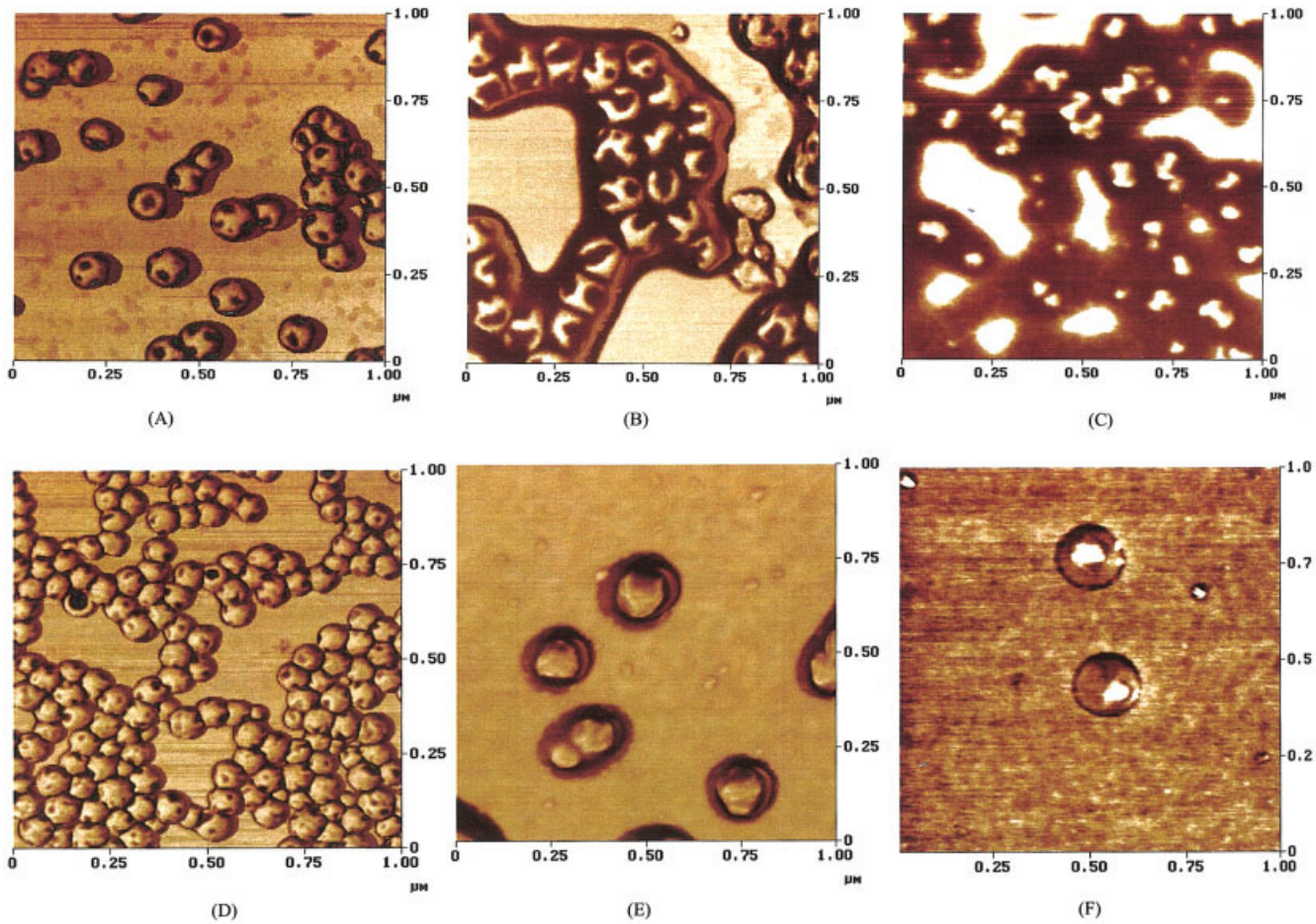

Figure 5 A phase image taken by AFM sample (A) I75/25, (B) I50/50, and (C) I25/75, (D) I75p/25, (E) I50p/50, and (F) I25p/75 on a field of view of 1×1 μm is shown.

ever, the contact area of the polymer/polymer interphase is not completely minimized, which is evident from the presence of multiple PBA domains on the surface. This effect must be due to kinetic limitations, which prevent full consolidation of the PBA domains. The fact that the hard-phase core material no longer exhibits a spherical shape, as proven before by Figure 4, is expected to be due to the T_g of the seed particles being about 40°C, which is less than the polymerization temperature. The KMORPH simulations also showed that, for this experiment, the second-stage polymer radicals are able to penetrate to a significant degree [Fig. 3(C)].

When the soft-phase content is increased (sample I50/50, I25/75), the bowls of the soft phase now become connected. This is expected based on the EQMORPH simulations in Figure 2(B), which show that the soft phase tends to partially cover the seed polymer, and this is more easily accomplished with larger amounts of the soft phase. Due to the very low T_g of the soft phase, the soft phase seen in Figure 5(B,C) is able to flow and spread around the hard-phase core material during the sample preparation step for AFM. The effect of an altered seed structure is now extremely pronounced. It seems that the hard phase still tends to stay at the polymer/water interface to a certain extent, in agreement with simulations. For the I25/75 [Fig. 5(C)] particles, the hard-phase structure no longer can be resolved from the single particle images. Indeed, there seems to be a tendency during the second-stage polymerization for the first-stage polymer to generate interface toward the water phase to decrease the polymer/polymer interfacial area.

In the second set of experiments, I75p/25, I50p/50, and I25p/75 [Fig. 5(D–F)], the T_g of the hard phase (119°C, pure PMMA) is increased above polymerization temperature. For the single I50p50 particles in Figure 5(E), we now see a very clear soft phase. This implies that due to the decreased mobility of the second-stage polymer radicals within the glassy first-stage material, a more core-shell-like structure was built as was predicted by the KMORPH simulations. No clear Dalmatian structure can be seen for I75p25 [Fig. 5(D)] which has a smaller amount of soft phase. A thin shell with some tendency of bowl-formation of PBA can only be assumed because it is technically not possible to resolve clearly a difference in material contrast or a topographic effect by AFM for this sam-

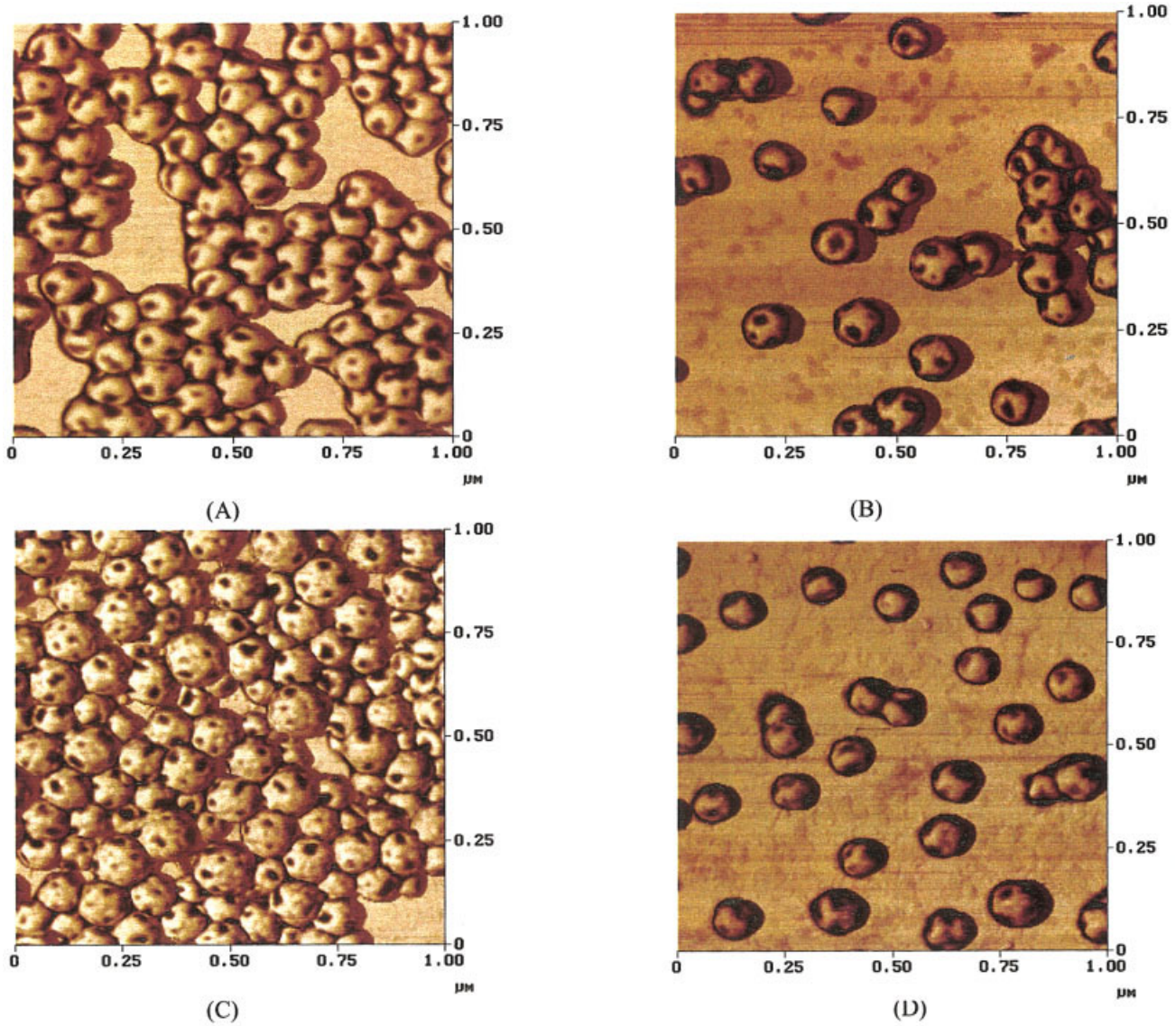

Figure 6 A phase image taken by AFM sample. (A) I75/25wo (no acrylic acid), (B) I75/25 (standard type), (C) I75a3/25 [3 parts per hundred monomers (pphm) acrylic acid in the first stage], and (D) I75/25a3 (3 pphm acrylic acid in the second stage) is shown. Field of view of 1×1 μm.

ple. In consequence, the structures shown in Figure 5(A, B) are a result of having a more partially engulfed structure. This is possible because the second-stage polymer radicals were able to penetrate significantly into the particles during polymerization in these experiments.

Influence of acrylic acid

The effect of acrylic acid on the single particle morphology is another focus of this work. In Figure 6(A–D), the results on the variation of acid concentration and distribution within the two stages are shown. For comparison, the image for the standard I75/25 particles is given in Figure 6(B). In a first step, the acrylic acid was removed (Table I, sample I75/25wo) from the recipe. The AFM phase image of the particles is shown in Figure 6(A). The Dalmatian-like domain structure remains. There are no significant differences compared to the morphology of the standard I75/25 particles. This is in agreement with the simulations, which predicted hemisphere morphologies for both experiments (EQMORPH) and similar levels of penetration (KMORPH). One may argue that the PBA contact area with the water is less in Figure 6(A) than in 6(B), which would agree with the trend predicted in Figure 2(A, B). However, this is only a minor point. In contrast to the latter results, the particle morphology is modified when the concentration of acrylic acid is increased and the distribution is varied. In Figure 6(C), the AFM phase image is shown for the I75a3/25 particles. Here, the whole amount of acrylic acid was polymerized in the first stage and the amount was doubled compared to the standard particles. We find

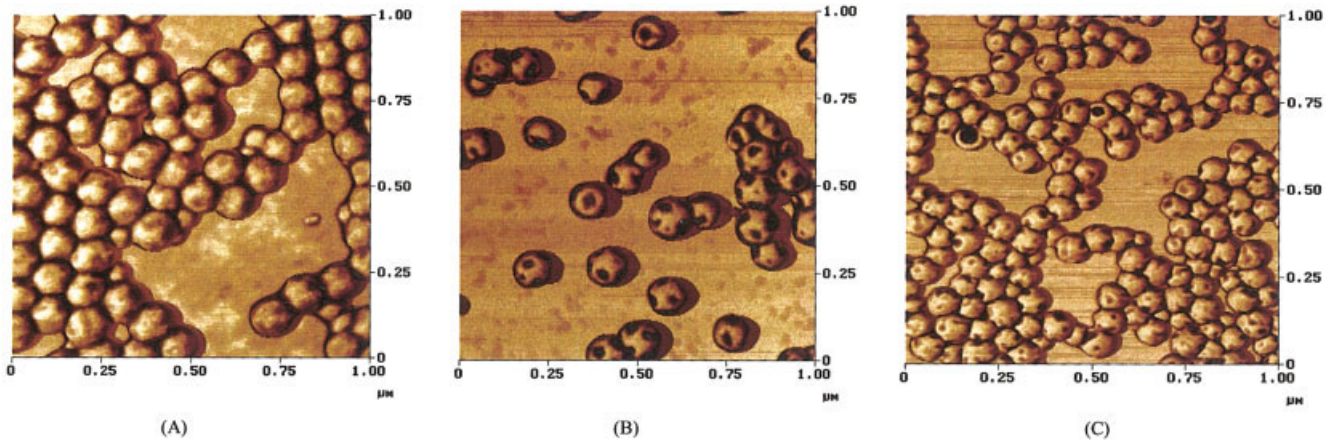

Figure 7 A phase image taken by AFM sample. (A) I75/25c (crosslinked shell), (B) I75/25 (standard type), and (C) I75p/25 (pure PMMA in the first stage) is shown. Field of view of 1 × 1 μm.

again the Dalmatian-like structure, but the formed bowls seem to be smaller in size and increased in number. This result is expected for two reasons: (1) from a thermodynamic point of view, the first-stage material is more hydrophilic and tends to orient toward the water phase, as indicated by the predicted inverted core-shell morphology, [Fig 2(C)]; (2) from a kinetic point of view, the ability of diffusion of the second-stage polymer radicals toward the interior of the particles, and the first stage polymer toward the water phase, is increased by the plastification effect due to swelling the seed polymer with water. When the whole amount of acrylic acid is put into the second stage, a core-shell structure (PBA shell) is expected. From the thermodynamic viewpoint, the argument is the same as in the previous case but the stage containing the acid is reversed. However, from a kinetic standpoint, the penetration of polymer radicals is now decreased by both the absence of plasticization of the seed polymer as well as the longer lengths for the entering second-stage radicals. These thermodynamic and kinetic effects are shown by the simulation results in Figures 2(D) and 3(B). This is what we found from the AFM phase images shown in Figure 6(D). Domains are no longer visible and it can be assumed that a thin shell is formed. These results are in accordance with those discussed in the previous section.

Effect of phase compatibility and crosslinking

In this section, the effects of phase compatibility (thermodynamic factor) and the polymer chain mobility (kinetic factor) are investigated. For comparison, the standard I75/25 is shown in Figure 7(B). Crosslinking of the second-stage polymer should result in less polymer chain mobility due to the higher molecular weight and significant chain entanglements of the second-stage polymer. Therefore, a core-shell-like structure may be expected. In the AFM phase image shown in Figure 7(A), no domain structure is visible, such as the type in Figure 7(B) for the standard I75/25 particles. As explained before in relation to Figure 5(D), it can only be assumed that a thin shell of PBA is present on these particles. Varying the chemical composition of the seed particles to pure PMMA has two effects. First, the phase compatibility is reduced and this increases the interfacial tension between the two polymer phases (thermodynamic effect). Second, the T_g of the seed is now well above the polymerization temperature, so that the diffusion of second-stage polymer radicals is very limited (kinetic effect). From the first argument, we would expect a hemisphere structure [Figure 2(E)] and from the second point of view a more core-shell-like structure [Figure 3(D)]. In Figure 7(C), the phase image of the sample I75p/25 is shown. Compared to the standard I75/25 particles, less soft domains are visible on the surface and the morphology appears to be more core-shell-like, as discussed previously in relation to Figure 6(D) for this same system. However, there is still a tendency for some bowl-formation even though the T_g of the PMMA is above polymerization temperature. This result suggests that the main driving force for the resulting structure is of kinetic origin.

Structure of dispersion films

From the point of view of application properties, the most crucial question is whether the morphology of the single particles is preserved during film formation and how film formation is related to the particle structure. As given in Table III, films of the samples I50/50, I25/75 and I50p/50, I35p/65, I25p/75 could be obtained at room temperature. All samples, with a phase ratio of 75% first stage and 25% second stage, are not suitable for applications at room temperature without using a coalescence agent. The soft-phase material is

TABLE III
Composition and Characteristics of the Corresponding Dispersion Film

Sample—Hard/soft (wt %)	T_g[a] (°C)	Film gloss[b] 20°/60°	Pendulum hardness[c] (s)	MFFT[d] (°C)
I75/25	49/−40	—	No film formation at 25°C	37
I50/50	50/−37	22/63	8	<0
I25/75	44/−42	45/79	4	<0
I75/25 wo	45/−45	—	No film formation at 25°C	38
I75a3/25	52/−42	—	No film formation at 25°C	>40
I75/25a3	46/−32	—	No film formation at 25°C	>40
I75/25 c	45/−26	—	No film formation at 25°C	>40
I75p/25	123/−39	—	No film formation at 25°C	>40
I50p/50	119/−3	58/77	28	6
I35p/65	120/−4	64/83	14	4
I25p/75	116/−3	58/83	9.4	0

[a] T_g as measured by differential scanning calorimetry.
[b] 200-μm film (wet), 24 h drying time, measured with a BYK Gardener Micro TRI gloss meter.
[c] 200-μm film (wet), 24 h drying time, according to DIN 53157, the time is given to stop an oscillating pendulum.
[d] According to ISO 2115 plastics.

not sufficient to provide a continuous soft phase in the film.

In Figure 8(A, C), AFM images of the surface of the corresponding dispersion films of I50/50 and I 25/75 are shown. From the picture of I50/50 in Figure 8(A), one can see that the structure of the hard phase is

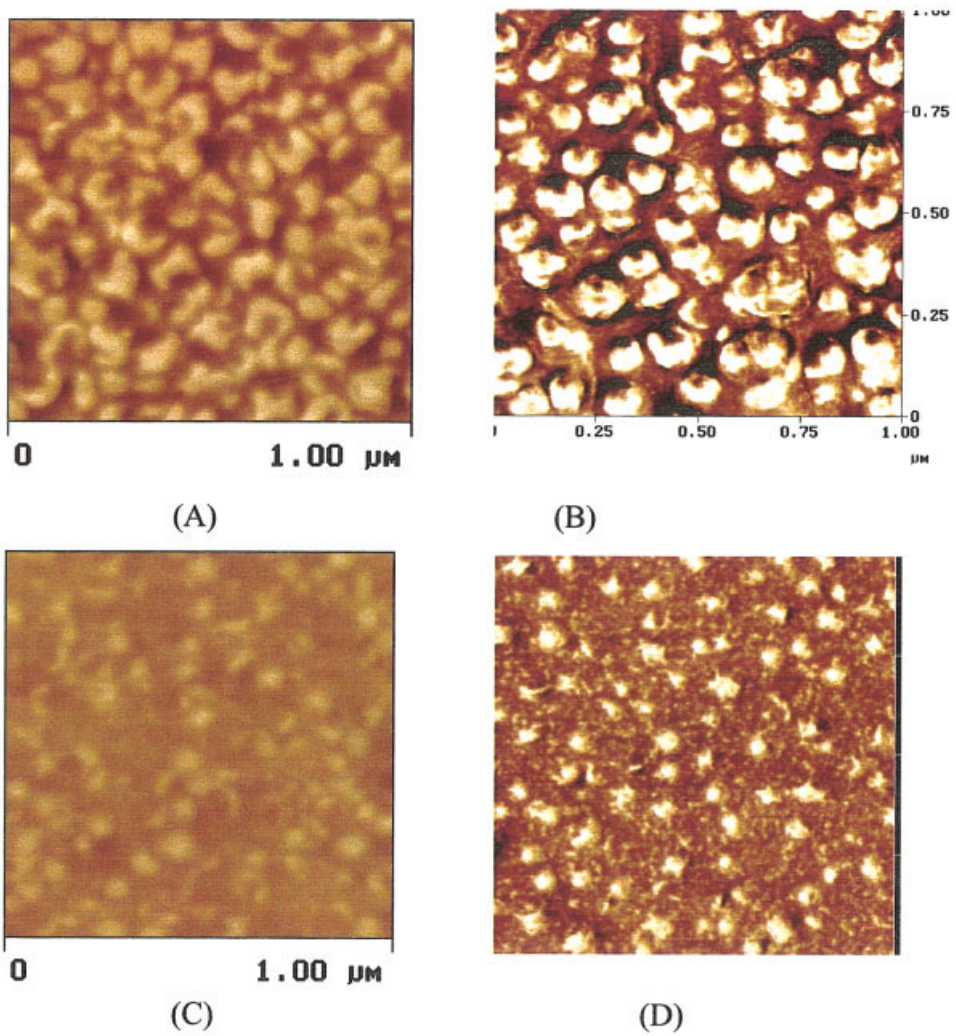

Figure 8 AFM images of the dispersion films of (A) I50/50 and (B) I50p/50, (C) I25/75 and (D) I25p/75. Field of view of 1×1 μm.

retained during film formation. In this material contrast image, the structure of the hard-phase material of the former seed particles is clearly visible. The soft-second stage material is now acting as a matrix within which the hard-phase structures are embedded. Because of this result, we can conclude that it is possible to draw some conclusions about the single-particle morphology from the film structure. This goes in line with our findings reported in ref. 18. From the AFM image for the I25/75 particles in Figure 8(C), we now get a better insight into the former single-particle morphology. From the material contrast image [Figure 8(D)], we conclude a more hemispheric-type particle structure, where the hard phases now form domains. Hence, at this phase ratio, the polymer/polymer interfacial tension seems to dominate over the polymer/water interfacial tension, causing a shift of the polymer/polymer contact area when the phase ratio is varied. Not surprisingly, increasing second-stage material decreases the surface roughness according to the topographic contract.

Figure 8(B, D) shows the AFM images of I50p/50 and I25p/75. The difference, compared to I50/50 and I25/75, is the increase in the T_g of the first-stage material. The effect is clearly visible by the modified film structure. For both samples, there is now a more core-shell-like structure due to the limited polymer chain mobility within the glassy PMMA phase.

Correlation to macroscopic properties

In Table III, the film gloss and the pendulum hardness of the film forming samples I50/50, I25/75 as well as I25p/75, I35p/65, and I50p/50 are given. The film gloss values of all samples do not vary significantly. As long as enough soft-phase material is present to guarantee a proper film formation, the film gloss is not strongly influenced by the phase ratio. This is in accordance with the observations for films of phase-separated dispersion particles with a soft core and a hard shell.[18] However, I50/50 quite clearly shows a lower film gloss, as compared to I50p/50. This can be attributed to the better phase compatibility of the hard and the soft phase of I50/50. In the case of I50p/50, there is a sharper interface between soft- and hard-phase material, which is due to the larger difference of polarity of both phases. Thus, the sharp separation of film-forming and non-film-forming material allows a better film formation for the I50p/50 system, which explains the higher gloss value. Apart from film gloss, the difference in pendulum hardness can be explained by the amount and the T_g of the hard-phase material. As would be expected, the samples with the higher amount of hard phase show higher values of pendulum hardness. Due to the T_g of the hard phase of I50/50 and I25/75 being more than 60°C lower than the three samples with pure PMMA as hard-phase material, it is quite obvious that the surface hardness of the former are lower even when the phase ratio is the same.

Comparison of the results

In this contribution, the hard-phase materials with T_g's of 40 or 119°C, respectively, were polymerized in a first step, followed by the soft-phase material. This is in contrast to ref. 18 and 6, where the sequence of polymerization of soft and hard phases (only pure MMA with a T_g of 119°C) was reversed. It is important to compare the differences in morphology of both systems, to understand the resulting impact on the macroscopic properties of the polymer films.

When the hard-phase material (pure MMA) is polymerized in the second stage, it covers the surface of the soft phase to a certain degree. With an increasing amount of hard phase, the surface coverage increases as well.[18] With small amounts of hard phase (up to about 30%), isolated islands on the soft phase are formed, while connected islands are created at hard-phase ratios higher than 30%. Thus, at a ratio of 50 soft/50 hard, no film formation of these particles occurs.[6] This is in contrast to the I50p/50 particles from this contribution, which are film forming. Comparing the particle morphology, it is quite obvious that when polymerizing the soft phase first, the hard phase covers nearly the whole surface of the particle. However, by polymerizing the hard phase first, much more soft phase is located at the interface with the water. Therefore, the soft phase can flow off the particles and form a continuous film. Thus, the order of polymerization has a strong impact on the particle morphology, which itself determines the macroscopic behavior, such as MFFT. This dependence on the order of polymerization has to be a kinetic factor because it does not have any effect on the interfacial tensions, which determine the thermodynamic driving forces. In the case of the I25/75 particles, the morphology does not seem to be very much different from the inversely produced particles with a pure MMA hard phase (75 soft/25 hard). In both cases, small islands of hard phase seem to be located on the surface of the soft phase. However, pendulum hardness of I25/75 (4s) is much less than for 75 soft/25 hard (28s), which can be related to the difference in T_g of the hard-phase material. Interestingly, I25p/75 is very much different from the inversely produced system, as the hard phase in that case is not located on the surface, but in the center of the particle. This was already explained by the high T_g of the pure PMMA, which hinders the diffusion of the soft phase toward the inside of the particle under polymerization conditions.

CONCLUSIONS

Structured latex particles have been synthesized via a two-step emulsion polymerization process. Two sets

of model dispersions were made. In the first the phase, ratio of high T_g seed to the low T_g shell was varied, which is the reverse of what was reported in ref. 18. In the second set, the phase compatibility was varied by changing the distribution of acrylic acid, crosslinking the shell, or varying the copolymer composition of the seed. The resulting structures were predicted based on simulation software tools developed at the University of New Hampshire. The single particle morphologies, as well as the surface structures of the corresponding films, have been characterized by AFM by using the tapping mode. The particle morphologies found are in excellent agreement with the predictions from simulation. Different experimental parameters were checked with respect to their impact on the final particle morphology. They can all be derived in a framework considering thermodynamic and kinetic aspects. In contrast to the work reported in ref. 18, the impact of kinetic effects is now much higher because of the fact that high T_g seed particles were used. Thus, the sequence of monomer feed is of major relevance for the morphology in such systems when one polymer phase is in, or almost in, the glassy state during polymerization process. This results in a different particle morphology for most of the particles with similar stage ratios and compositions. For the hard/soft series, the macroscopic properties of the dispersion films, such as MFFT and pendulum hardness, could be attributed to their structure, which is in accordance with our findings reported in ref. 18. Thus, for comparable amounts of high T_g polymer phase in dependence of the feeding sequence, taking advantage of the kinetic control on the formation of the final morphology during polymerization, different application properties can be tailored to fulfill the requirements in different fields of applications.

The skillful experimental assistance of Mr. Sander, Mr. Kren (AFM), Mrs. Langendörfer, and Mr. Wageck (synthesis) is gratefully acknowledged. J.M.S. and D.C.S. are thankful for the financial support from the University of New Hampshire Latex Morphology Industrial Consortium (ATOFINA, Neo-Resins, Mitsubishi Chemical, UCB Chemicals).

References

1. Schuler, B.; Baumstark, R.; Kirsch, S.; Pfau, A.; Sandor, M.; Zosel, A. Prog Org Coat 2000, 40(1–4), 139.
2. Baumstark, R.; Kirsch, S.; Schuler, B.; Pfau, A. Farbe Lack 2000, 106, 125.
3. Kirsch, S.; Pfau, A.; Hädicke, E.; Leuninger, J. Prog Org Coat 2002, 45, 193.
4. Pfau, A.; Sander, R.; Kirsch, S. Langmuir 2002, 18, 2280.
5. Sundberg, E. J.; Sundberg, D.C. J Appl Polym Sci. 1993, 47, 1277.
6. Kirsch, S.; Landfester, K.; Shaffer, O.; El-Aasser, M. S. Acta Polym 1999, 50, 347.
7. Sundberg, D. C.; Casassa, A. P.; Pantazopoulos, J.; Muscato, M. R.; Kronberg, B.; Berg, J. J Appl Polym Sci 1990, 41, 1425.
8. Chen, Y. C.; Dimonie, V.; El-Aasser, M. S. J Appl Polym Sci. 1992, 45, 487.
9. Lee, S.; Rudin, A. J Polym Sci, Part A: Polym Chem 1992, 30, 2211.
10. Lee, S.; Rudin, A. J Polym Sci, Part A: Polym Chem 1992, 30, 2211.
11. Durant, Y. G.; Sundberg, D. C. Macromol Symp 1995, 92, 43.
12. Durant, Y. G.; Sundberg, D. C. ACS Symposium Series 663; American Chemical Society: Washington, DC, 1997; p 44.
13. Kirsch, S.; Dörk, A.; Bartsch, E.; Sillescu, H.; Landfester, K.; Spiess, H.W.; Mächtle, W. Macromolecules 1999, 32, 4508.
14. Stubbs, J.; Karlsson, O.; Jönsson, J. E.; Sundberg, E. S.; Durant, Y. G.; Sundberg, D. C. Colloids Surf A 1999, 153, 255.
15. Vorweg, L.; Gilbert, R. G. Macromolecules 2000, 33 (18), 6693.
16. Kirsch, S.; Pfau, A.; Landfester, K.; Shaffer, O.; El-Aasser, M. S. Macromol Symp 2000, 151, 413.
17. Karlsson, O.; Hassander, H.; Wesslen, B. J Appl Polym Sci 1997, 63, 1543.
18. Kirsch, S.; Pfau, A.; Stubbs, J.; Sundberg, D. Colloids Surf A 2001, 183–185, 725.
19. Durant, Y. G.; Sundberg, D. C. J Appl Polym Sci. 1995, 58, 1607.
20. Karlsson, O. J.; Stubbs, J. M.; Carrier, R. H.; Sundberg, D. C. Polym React Eng, to appear.
21. Stubbs, J. M.; Karlsson, O. J.; Carrier, R. H.; Sundberg, D. C. Prog Colloid Polym Sci, to appear.
22. Zhhong, Q.; Innis, D.; Kjoller, K.; Elings, V. B. Surf Sci. 1993, 290, L688.
23. Magonov, S. N.; Elings, V.; Whangbo, M.-H. Surf Sci 1997, 375, L385.
24. Winzor, C. L.; and Sundberg, D. C. Polymer 1992, 33, 3797.
25. Dong, Yan; Sundberg, Donald C. J Colloid Interface Sci 2003, 258(1), 97.
26. Souheng, Wu. Polymer Interface and Adhesion; Marcel Dekker: New York, 1982; p 102.
27. Karlsson, O. J.; Stubbs, J. M.; Karlsson, L. E.; Sundberg, D. C. Polymer 2001, 42, 4915.
28. Lyons, R. A.; Hutovic, J.; Piton, M. C.; Christie, D. I.; Clay, P. A.; Manders, B. G.; Kable, S. H.; Gilbert, R. G. Macromolecules 1996, 28, 1918.
29. Dong, Y.; and Sundberg, D. Macromolecules, 2002, 35, 8185.
30. Lee, D.; Walker, L.; Kan, C. Macromol Symp 1997, 118, 267.